©A. Caspari et al. Page 1 of 33

A Wave Propagation Approach for Reduced Dynamic Modeling of

2 Distillation Columns: Optimization and Control

- $\,$ Adrian Caspari a, Christoph Offermanns a, Anna-Maria Ecker d, Martin Pottmann d, Gerhard Zapp d, Adel
- 4 Mhamdi^a, Alexander Mitsos^{b,a,c,*}
- ⁵ Process Systems Engineering (AVT.SVT), RWTH Aachen University, 52074 Aachen, Germany
- ⁶ JARA-CSD, 52056 Aachen, Germany
- ⁷ Energy Systems Engineering (IEK-10), Forschungszentrum Jülich, 52425 Jülich, Germany
- ⁸ Linde Aktiengesellschaft, Linde Engineering, 82049 Pullach, Germany
- Abstract: Reduced models enable real-time optimization of large-scale processes. We propose a reduced model of distillation columns based on multicomponent nonlinear wave propagation [1]. We use a non-10 linear wave equation in dynamic mass and energy balances. We thus combine the ideas of compartment modeling and wave propagation. In contrast to existing reduced column models based on nonlinear wave propagation, our model deploys a hydraulic correlation. This enables the column holdup to change as 13 load varies. The model parameters can be estimated solely based on steady-state data. The new transient 14 wave propagation model can be used as a controller model for flexible process operation including load 15 changes. To demonstrate this, we implement full-order and reduced dynamic models of an air separation process and multi-component distillation column in Modelica. We use the open-source framework 17 DyOS for the dynamic optimizations and an Extended Kalman Filter for state estimation. We apply the reduced model in-silico in open-loop forward simulations as well as in several open- and closed-loop optimization and control case studies, and analyze the resulting computational speed-up compared to using full-order stage-by-stage column models. The first case study deals with tracking control of a single air separation distillation column, whereas the second one addresses economic model predictive control of an entire air separation process. The reduced model is able to adequately capture the transient column 23 behavior. Compared to the full-order model, the reduced model achieves highly accurate profiles for the 24 manipulated variables, while the optimizations with the reduced model are significantly faster, achieving more than 95% CPU time reduction in the closed-loop simulation and more than 96% in the open-loop 26 optimizations. This enables the real-time capability of the reduced model in process optimization and control.
- Keywords: reduced distillation model, wave propagation, dynamic optimization, model predictive con-
- trol, large-scale process, output feedback control

E-mail: amitsos@alum.mit.edu

^{*} corresponding author: A. Mitsos, AVT Process Systems Engineering, RWTH Aachen University, 52074 Aachen, Germany

1 Introduction

The need for reduced models in transient process operation is well-known [2]. They enable a higher computational efficiency than full-order models, thus allowing online optimization of large-scale systems [2, 3], e.g., for air separation units (ASUs) [4, 5]. Reduced models should capture the main physicochemical effects mechanistically in order to obtain good extrapolation capabilities in an adequate region of the state-space. This in turn results in reducing experimental effort for model building compared to black-box models [2]. Distillation columns are ubiquitous in process engineering with applications spanning over broad fields including, e.g., natural gas [6] and ASUs [7]. Modeling distillation columns typically leads to large-scale models, so that there is a need for model reduction. Common model reduction methods for 10 distillation columns are based on collocation approaches [8, 9, 10], compartmentalization [11, 12, 13], 11 and wave propagation [14, 15, 16, 17, 1], and all of them have been applied to ASUs. Cao et al. [10] used the collocation approach for rectification columns for dynamic simulation of a large-scale ASU and showed that the reduced model achieves high accuracy. They demonstrated a reduction in model size by up to 72% and simulation time reductions of up to 63%. Later, they used collocation column 15 models for dynamic offline optimization of an ASU for nitrogen production [18]. Bian et al. [13] applied 16 a compartmentalization approach to an ASU and concluded that the reduced model admitted a high 17 accuracy and a significant reduction of the number of differential states compared to a stage-by-stage full-18 order model (FOM). However, it did not produce a significant decrease in computational time for open-19 loop forward simulation. Recently, we extended the compartmentalization approach by a data-driven component, where the solution of the algebraic equation system of the compartments is approximated 21 using artificial neural networks (ANN) [11]. In an application to an ASU, we showed that the conventional compartment model reduction approach leads to an increase in the computational time for dynamic offline optimization, whereas our proposal leads to a reduction in computational time for dynamic offline 24 optimization of 93-97%. Later, we used the ANN-based compartment model in a closed-loop simulation, applying nonlinear model predictive control (NMPC) with a suboptimal fast-update method [7], achieving 26 CPU time reductions for the dynamic optimizations of up to 94% compared to optimizations with the 27 FOM in [4]. 28 The nonlinear wave propagation approach for model reduction uses the observation that the temper-29 ature and concentration profiles in a distillation column can be described by waves moving along the column. Indeed, the system of partial-differential equations describing the concentration profile in a col-

©A. Caspari et al. 2 Page 2 of 33

umn can be solved analytically under certain assumptions and the resulting solution is a nonlinear wave

[1]. Although derived for a packed column, the nonlinear wave equations can also be used to described the profiles of a stage column [1]. Gilles and Retzbach [14, 15] presented a simple wave propagation model for a binary distillation column. However, the model can only represent sharp, i.e., discontinuous temperature and concentration profiles for binary mixtures or mixtures which behave as quasi-binary systems.

Marquardt [19] overcame the restriction to sharp profiles and developed a nonlinear wave propagation model for a binary distillation column. He used different spatial basis functions and time-varying quasistationary wave shape parameters, resulting in a linear differential-algebraic system of equations as a reduced model. He claimed that the distributed model is also valid for a stage-by-stage model even in case of small number of stages. Marquardt and Amrhein [20] presented a wave propagation model for a binary distillation column where the nonlinear wave is approximated by a piecewise affine profile. Based on the nonlinear wave propagation model for binary systems [19], Kienle [1, 21] presented a generalization of the nonlinear wave propagation models for multicomponent systems.

Wave propagation models offer several advantages making them attractive as reduced model for 14 optimization and control. As opposed to collocation and compartment models, they do not rely on 15 the selection of an appropriate number and location of collocation points and compartments. In the collocation approach, the collocation points have to be selected manually as in [10] or automatically, 17 e.g., [22], which requires the solution of computational intensive dynamic optimization problems with binary decision variables [10]. The compartments in the compartment model reduction approach have to be selected manually [12, 13, 11]. In contrast, reduced models based on wave propagation use only 20 steady-state data of a more detailed column model or plant operation data, whereas collocation and 21 compartment models are pure model reduction techniques needing more detailed dynamic models as 22 they require variable values from the inside of the column as opposed to input-output data. Thus, these 23 approaches require trajectories, i.e., time dependent data from dynamic simulation of these models for 24 generation [10, 13, 11]. The hybrid mechanistic-data driven compartment modeling approach further needs the exact a-priori knowledge of the ranges of the input variables for the compartments in order to train the regression model to the solution of the algebraic equations of each compartment [11]. As opposed to the other model reduction approaches, the size of wave propagation models is independent of the number of trays of the real column or detailed column model. On the other hand, wave propagation models are technically restricted to near ideal thermodynamic mixtures [1], which limits their applicability. However, they can still by applied for optimization and control for a broad range of mixtures and even 31 when the given assumptions [1] are violated, as we show in this work.

©A. Caspari et al. 3 Page 3 of 33

Wave propagation models have been applied for modeling, simulation, and model-based process control. Balasubramahanya and Doyle [23] used a wave propagation model for design of a nonlinear controller and and its comparison to two linearized controllers. Kienle et al. [21] embedded the wave equations from their previous work [1] in a dynamic mass and a quasi-stationary energy balance as a reduced model that captures variable flow rates and constant volumetric holdups. The constant volumetric holdup assumptions require the calculation of the volume at every column stage, which increases the computational time when the model is used in optimization. Moreover, they concluded that further work is required to obtain a good performance for interlinked systems or the application of low-order models for process control like dynamic optimization of transient operation, e.g., with setpoint changes. Therefore, we target a wave propagation based model that can be used in transients process operation with changing setpoints. Zhu [24] used a nonlinear wave propagation model for a binary cryogenic distillation column for nitrogen 11 purification. They compared the reduced model based on wave propagation with a FOM and found 12 satisfactory accuracy over a large operating range. Later, they used the binary wave propagation model 13 for state estimation and model predictive control of a single air separation distillation column [25]. They used the control strategy with a wave propagation model to keep the oxygen impurity of the nitrogen 15 product stream constant despite the presence of disturbances. The wave position and wave propagation model parameters were estimated online.

Grüner et al. [26] used the model of Kienle [1] for NMPC of a single binary and single multicomponent distillation column. They used NMPC to keep the wave at the nominal position in the presence of disturbances and used a specialized observer to provide the initial states to the NMPC. They performed 20 a closed-loop case study for a binary and an offline dynamic optimization for a ternary distillation 21 column. Schwartzkopf [27] also used the model of Kienle [1] for NMPC of a single binary and ternary 22 distillation column. He deployed NMPC to keep the wave fronts at a specified position in the presence 23 of disturbances and performed a closed-loop control case-study for a binary distillation column and an 24 offline dynamic optimization for a ternary distillation column. He concluded that wave propagation based models are suitable as controller models for NMPC. Hankins [28] developed a multicomponent nonlinear wave propagation model with variable molar flows. Using the assumption that the molar holup and enthalpy are linear functions of the concentration in the column he derived the solution for the velocity of a constant pattern wave that includes enthalpy and holdup effects. Fu and Liu [29] used and analyzed a nonlinear wave propagation model for a heat integrated air separation column. First, they analyzed their previously developed natural wave velocity [30]. Then, they used the same nonlinear wave propagation 31 concentration trial function for the entire column as has been used and derived earlier by [19, 1]. They

©A. Caspari et al. 4 Page 4 of 33

21

22

23

24

25

31

showed the accuracy of the model they used compared to a FOM. Fu and Liu [31] used a simplified wave propagation model based on their earlier work [29] for a heat integrated air separation column as controller model within a generalized generic model control scheme.

Despite this wide range of applications, several aspects of wave propagation models have not yet been adressed. These aspects include the usage of wave propagation models for NMPC of entire process flowsheets. Wave propagation models have further not been used for closed-loop control of multicomponent distillation columns with NMPC. In addition, wave propagation models have not been used for transients process operation, e.g., the tracking of changing product flow setpoints or eonomically optimized process operation in the context of demand side management, e.g., [32]. Indeed, wave propagation models are derived only for constant flowrates and holdups. However, in the case of substantial load changes, the flowrates and hence holdups change substantially. This would give a nonphysical behavior of standard 11 wave propagation model. Therefore, we propose to embed the propagation model of Kienle [1] in dynamic 12 balance equations and add hydraulic correlations enabling the model to capture also transient column 13 behavior. Hence, our proposal combines the ideas of the compartment model reduction approach and the 14 wave propagation model approach; we describe the dynamics of a distillation column by one compartment 15 and describe the concentration profiles in the compartment by the nonlinear wave equations of Kienle [1]. We use the proposed model in offline optimization and control case studies of a single distillation 17 column and an entire ASU. We analyze the performance of the reduced column model with respect to computational time and accuracy in comparison with a standard FOM and show that the model is able to adequately predict the physical load change behavior. 20

Thus, our work addresses several new asepcts. While [26, 27, 31] used NMPC with the wave propagation model for disturbance rejection, we use a wave propagation based model that is modified for the application in transients process operation and apply it for NMPC of a single column and of an entire ASU flowsheet. In contrast to [25], we use NMPC for the optimal transient operation of a single distillation column and an entire ASU based on a modified wave propagation model. We achieve satisfactory open- and closed-loop performance without estimating and changing the wave propagation model parameters online. Opposed to [28], we include holdup effects by using a hydraulic correlation for the entire column and embed a nonlinear wave propagation model that has been derived for constant holdups, and include enthalpy effects by considering the average enthalpy of the column. While Hankins [28] gave the application of the proposed model in process control in the outlook, we demonstrate the application in optimization and control.

The remainder of the article is structured as follows. First, we summarize the nonlinear wave prop-

©A. Caspari et al. 5 Page 5 of 33

- agation model of Kienle [1] in Section 2.1, give the reduced column model that we propose in Section
- 2 2.2, and present the dynamic optimization problem formulation and process control strategy applied in
- Section 2.3. We show the results of open-loop forward simulations, offline dynamic optimizations and of
- the closed-loop simulations in Section 3. Finally, we draw conclusions in Section 4.

s 2 Reduced Model Based on Wave Propagation

- ⁶ We use the nonlinear wave propagation model of Kienle [1] as basis for our reduced column model. We
- ⁷ therefore summarize the model of Kienle [1] before presenting the reduced model we propose.

8 2.1 Nonlinear Wave Propagation Model

Kienle [1] derived wave equations for the concentration profiles in a column assuming: (i) molar flow rates and densities in both phases are constant in time and uniform in space, (ii) negligible axial dispersion, (iii) thermal equilibrium between the phases at each position along the column, and (iv) the pressure is constant in time and uniform in space. Kienle derives wave equations for two limiting cases of the spatially distributed mass balance equations: the steady-state solution and the constant pattern shape solution, i.e., a wave with constant shape and constant velocity. The derivations show that both cases are described by the same functional expression. Therefore, the wave propagation model is assumed to be valid also during transient operation [1]. In the multicomponent case with N_c species, the concentration profiles can be described using $N_c - 1$ wave equations. The wave equations of the wave k for the liquid and vapor molar fractions are

$$x_i(\xi^{(k)}) = x_i^{(k)} + \frac{x_i^{(k+1)} - x_i^{(k)}}{1 + \exp(-\rho^{(k)}\xi^{(k)})},\tag{1}$$

$$y_i(\xi^{(k)}) = f_i(\boldsymbol{x}^{(k)}) + \frac{f_i(\boldsymbol{x}^{(k+1)}) - f_i(\boldsymbol{x}^{(k)})}{1 + \exp(-\rho^{(k)}\xi^{(k)})},$$
(2)

where the model variable $\rho^{(k)}$ is defined by

$$\rho^{(k)} = \frac{B \sum_{l=1}^{N_c - 1} \left((\alpha_l - 1)(x_l^{(k+1)} - x_l^{(k)}) \right)}{1 + \sum_{l=1}^{N_c - 1} \left((\alpha_l - 1)(x_l^{(k+1)} + x_l^{(k)}) \right) / 2}$$
(3)

and

$$f_i(\mathbf{x}) = \frac{\alpha_i x_i}{1 + \sum_{l=1}^{N_c - 1} (\alpha_l - 1) x_l}.$$
 (4)

©A. Caspari et al. 6 Page 6 of 33

10

Therein, x_i is the liquid phase molar fraction of species i, y_i the vapor phase molar fraction of species i, α_i denote the relative volatilities with respect to a reference species, $x_i^{(k)}$ and $x_i^{(k+1)}$ are the asymptotic molar fractions of species i for the wave k, B could be interpreted as the number of theoretical stages or estimated as a parameter as we do in this work. $\xi^{(k)}$ is the wave coordinate of wave k moving with the velocity $w^{(k)}$: $\xi^{(k)} = z - s^{(k)} = z - w^{(k)}t$, where $s^{(k)}$ is the position of wave k, $z \in [0,1]$ is the scaled coordinate along the column length and t is the time. $s^{(k)}$ follow from the mass balances and $w^{(k)}$ can be calculated based on $s^{(k)}$.

The concentration profiles in the column are obtained by linear superposition of the nonlinear waves:

$$x_{i}(z, s^{(1)}, ...s^{(N_{c}-1)}) = x_{i}^{(1)} + \sum_{k=1}^{N_{c}-1} \frac{x_{i}^{(k+1)} - x_{i}^{(k)}}{1 + \exp(-\rho^{(k)}(z - s^{(k)}))}, i \in \{1, ..., N_{c} - 1\},$$
 (5)

$$y_i(z, s^{(1)}, ...s^{(N_c - 1)}) = f_i(\boldsymbol{x}^{(1)}) + \sum_{k=1}^{N_c - 1} \frac{f_i(\boldsymbol{x}^{(k+1)}) - f_i(\boldsymbol{x}^{(k)})}{1 + \exp\left(-\rho^{(k)}(z - s^{(k)})\right)}, i \in \{1, ..., N_c - 1\},$$
(6)

where $s^{(k)}$ is the front position of wave k: $s^{(k)} = w^{(k)}t$. The asymptotic states $x_i^{(k)}$ and $x_i^{(k+1)}$ can be calculated for given $x_i^{(1)}$ and $x_i^{(N_c)}$ from the Ranking-Hugoniot condition:

$$\frac{f_1(\boldsymbol{x}^{(k+1)}) - f_1(\boldsymbol{x}^{(k)})}{x_1^{(k+1)} - x_1^{(k)}} = \dots = \frac{f_{N_c - 1}(\boldsymbol{x}^{(k+1)}) - f_{N_c - 1}(\boldsymbol{x}^{(k)})}{x_{N_c - 1}^{(k+1)} - x_{N_c - 1}^{(k)}}.$$
 (7)

The asymptotic values at the lower and upper boundary $x_i^{(1)}$ and $x_i^{(N_c)}$ follow from the boundary conditions of the column section with

$$x_i(z=1) = x_{i,\text{in}},\tag{8}$$

$$y_i(z=0) = y_{i,in}, (9)$$

where $x_{i,\text{in}}$ and $y_{i,\text{in}}$ are the mole fractions of the liquid and vapor inlet streams, respectively.

The full wave model consists of equations (1)-(9). It is a set of algebraic equations that can be embedded in balance equations to form a reduced column model. There are $N_c - 1$ more variables than equations. $N_c - 1$ mass balance equations can be added to the nonlinear wave propagation equations to complete the nonlinear system of equations, as we show in the Section 2.2. Thus, the total component holdups in the column is connected to the $N_c - 1$ unknown wave positions $s^{(k)}$.

Kienle et al. [1, 21] embedded the wave equations in balance equations assuming constant holdups and volumes, respectively. As these assumptions either lead to nonphysical model behavior during load

©A. Caspari et al. 7 Page 7 of 33

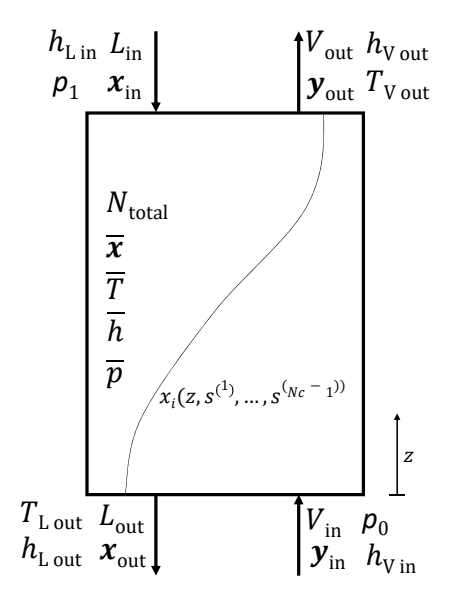


Fig. 1: Schematic illustration of Transient Wave Propagation Mode (TWPM). The TWPM is a combination of a compartment model and a wave propagation model. The profiles of component concentrations in the compartment are described by wave propagation equations. The molar fractions \bar{x} , temperature \bar{T} , \bar{h} , and enthalpy \bar{p} are averaged over the column height.

change or additional computational load due to volume calculations, we propose a new reduced model

using the wave equations, which we present in the following section.

2.2 Reduced Column Model for Transient Operation Using Nonlinear Wave

Propagation Functions

We target a reduced column model which is able to adequately represent load changes and to capture

the resulting load-dependent column holdup. In addition, we target a reduced model which is physically-

based and allows for extrapolation. We aim for it to use parameters that can be estimated solely from

steady-state data obtained from a FOM. We denote our proposed reduced column model as transient

wave propagation model (TWPM). The TWPM is illustrated in Fig. 1. The model is developed using

the following ideas: (i) we use a dynamic mass balance for the overall column with a global hydraulic

 $_{11}$ correlation using the parameter k_d connecting liquid outlet flowrate and total column holdup. This

enables the model to represent the column behavior also during load changes. The type of hydraulic

correlation depends on the characteristic dynamic behavior of the column we want to be approximated

by the reduced model. In contrast to standard FOMs, e.g., [33, 34], we use the linear hydraulic correlation

©A. Caspari et al. 8 Page 8 of 33

- 1 for the overall column and not for every stage. We thus assume equally-distributed, time-varying mass
- 2 holdups in the column. (ii) Similar to [1], we assume that the flowrates and holdups are quasi-stationary.
- 3 (iii) Since the wave equations in [1] result from different limiting steady-state cases, the model in [1]
- 4 is postulated to be valid during the transient operation between these cases. As these assumptions are
- 5 satisfied for the TWPM at the steady-states as well, we also assume the model to be valid during transient
- operation. (iv) We assume quasi-stationarity for the enthalpy \bar{h} and (v) negligible vapor holdup.
- We use the integral total mole balance

$$\frac{\mathrm{d}N_{\text{total}}}{\mathrm{d}t}(t) = L_{\text{in}}(t) - L_{\text{out}}(t) + V_{\text{in}}(t) - V_{\text{out}}(t) \tag{10}$$

- with the liquid inlet flowrate $L_{\rm in}$, the liquid outlet flowrate $L_{\rm out}$, the vapor inlet flowrate $V_{\rm in}$, the vapor
- outlet flowrate V_{out} , and the component mole balances

$$N_{\text{total}}(t) \frac{d\bar{x}_{i}}{dt}(t) = L_{\text{in}}(t) \left(x_{\text{in},i}(t) - \bar{x}_{i}(t) \right) - L_{\text{out}}(t) \left(x_{\text{out},i}(t) - \bar{x}_{i}(t) \right) + V_{\text{in}}(t) \left(y_{\text{in},i}(t) - \bar{x}_{i}(t) \right) - V_{\text{out}}(t) \left(y_{\text{out},i}(t) - \bar{x}_{i}(t) \right), i \in \{1, ..., N_{c} - 1\},$$
(11)

where $x_{\text{in},i}$ is the liquid inlet mole fraction of component i, $x_{\text{out},i}$ is the liquid outlet mole fraction of component i, $y_{\text{in},i}$ is the vapor inlet mole fraction of component i, and $y_{\text{out},i}$ is the vapor outlet mole fraction of component i. The average mole fraction \bar{x}_i of component i is calculated based on the nonlinear wave equation:

$$\bar{x}_i(t) = \int_{z=0}^1 x_i(z, s^{(1)}(t), ..., s^{(N_c-1)}(t)) dz, i \in \{1, ..., N_c - 1\}$$
(12)

and the hydraulic correlation

$$L_{\text{out}}(t) = k_d N_{\text{total}}(t), \tag{13}$$

where $k_{\rm d}$ connects the liquid outlet stream $L_{\rm out}$ and the overall column holdup $N_{\rm total}$. As the wave propagation model is exact for systems that satisfy the assumptions of Kienle [1] given above, the steadystate prediction of the TWPM is perfect in this case. The dynamic bevahior of the TWPM depends on the hydraulic correlation used and can be modified by adjusting the parameter $k_{\rm d}$. Other hydraulic correlations than (13) could be used, e.g., the one used by Raghunathan and Biegler [35]. The overall hydraulic correlation to describe the dynamic behavior of the overall column combined with the mass and energy balance of the column is the concept taken from compartment modeling. The component mass balances (11) allow for varying flowrates. The outlet concentrations are calculated using the wave

©A. Caspari et al. 9 Page 9 of 33

equations (5)-(6) with

$$x_{\text{out},i}(t) = x_i(z=0,t)$$

$$y_{\text{out},i}(t) = y_i(z=1,t)$$
(14)

We use a dynamic energy balance for the overall column with assumption (iv):

$$\frac{\mathrm{d}N_{\text{total}}}{\mathrm{d}t}(t)\bar{h}(t) = L_{\text{in}}(t)h_{\text{L,in}}(t) - L_{\text{out}}(t)h_{\text{L,out}}(t) + V_{\text{in}}(t)h_{\text{V,in}}(t) - V_{\text{out}}(t)h_{\text{V,out}}(t), \tag{15}$$

- where $h_{L,in}$ is the enthalpy of the liquid inlet stream, $h_{L,out}$ the enthalpy of the liquid outlet stream,
- $_4$ $h_{
 m V,in}$ the enthalpy of the vapor inlet stream, $h_{
 m V,out}$ is the enthalpy of the vapor outlet stream. With
- assumption (iv), the average enthalpy \bar{h} is calculated based on average temperature, pressure, and molar
- 6 fraction

$$\bar{h}(t) = h_{L}(\bar{T}(t), \bar{\boldsymbol{x}}(t), \bar{p}(t)),$$

$$\bar{T}(t) = (T_{V,\text{out}}(t) + T_{L,\text{out}}(t))/2,$$

$$h_{L,\text{out}}(t) = h_{L}(T_{L,\text{out}}(t), \boldsymbol{x_{\text{out}}}(t), p_{0}(t)),$$

$$h_{V,\text{out}}(t) = h_{V}(T_{V,\text{out}}(t), \boldsymbol{y_{\text{out}}}(t), p_{1}(t)),$$

$$\bar{p}(t) = (p_{0}(t) + p_{1}(t))/2,$$

$$(16)$$

where $h_{\rm L}: \mathbb{R} \times \mathbb{R}^{N_c} \times \mathbb{R} \to \mathbb{R}$ and $h_{\rm V}: \mathbb{R} \times \mathbb{R}^{N_c} \times \mathbb{R} \to \mathbb{R}$ are suitable liquid and vapor enthalpy models, \bar{T} is the average temperature, and p_0 and p_1 are the bottom and top pressures, and $T_{L,out}$ and $T_{V,out}$ are the temperatures of the outlet liquid and vapor stream. The reduced column model we propose consists of the equations (1)-(16). It is a semi-explicit DAE with differential index 1. We model the top and bottom stage of the column as equilibrium stages, so that saturated liquid or vapor enters the nonlinear wave 11 propagation model at the top and bottom, respectively, even when the feed streams ar not saturated. 12 The TWPM applies to a single column section. More complex situations, e.g., with several side streams, 13 can be handled by multiple TWPMs. Two TWPMs can be coupled by one equilibrium stage with feed 14 streams entering or side streams being withdrawn. We calculate p_0 and p_1 using a constant pressure drop 15 of the column height. Other correlations could be also be used. However, the pressure does not affect 16 the concentration profiles from the wave propagation model. It only affects the feed stages modeled as equilibrium stages or intermediate equilibrium stages used to obtain variables from the inside of the column, such es temperature values from the column inside.

©A. Caspari et al. 10 Page 10 of 33

2.3 Formulation of Dynamic Optimization Problems and Process Control Scheme

- This section presents the dynamic optimization problem formulation and the process control scheme that
- we use in the case studies as an application of the TWPM. We consider dynamic optimization problems
- of the form

2

$$\min_{\boldsymbol{x},\boldsymbol{y},\boldsymbol{u}} \Phi(\boldsymbol{x}(t_f))$$
s.t. $\boldsymbol{M}\dot{\boldsymbol{x}}(t) = \boldsymbol{f}(\boldsymbol{x}(t),\boldsymbol{y}(t),\boldsymbol{u}(t),\boldsymbol{p}(t))$

$$\boldsymbol{0} = \boldsymbol{g}(\boldsymbol{x}(t),\boldsymbol{y}(t),\boldsymbol{u}(t),\boldsymbol{p}(t))$$

$$\boldsymbol{x}(t_0) = \boldsymbol{x_0}$$

$$\boldsymbol{0} \geqslant \boldsymbol{c}(\boldsymbol{x}(t),\boldsymbol{y}(t),\boldsymbol{u}(t),\boldsymbol{p}(t)), t \in \mathcal{T}$$
(17)

where $\boldsymbol{x}:\mathcal{T}\to\mathbb{R}^{N_x}$ are the differential states, e.g., molar holdups in the column, $\boldsymbol{y}:\mathcal{T}\to\mathbb{R}^{N_y}$ are the algebraic states, e.g., product concentrations, $u: \mathcal{T} \to \mathbb{R}^{N_u}$ are the manipulated variables (MVs), $p: \mathcal{T} \to \mathbb{R}^{N_p}$ are the parameters, e.g., changing setpoints or electricity prices, $f: \mathcal{X} \to \mathbb{R}^{N_x}, g: \mathcal{X} \to \mathbb{R}^{N_y}$ are the equations defining the index 1 DAE, $\mathcal{X} = \mathbb{R}^{N_x} \times \mathbb{R}^{N_y} \times \mathbb{R}^{N_u} \times \mathbb{R}^{N_p}$, $\mathcal{T} = [t_0, t_f]$, and $\mathbf{c} : \mathcal{X} \to \mathbb{R}^{N_g}$ are path and terminal constraints, and $\mathbf{M} \in \mathbb{R}^{N_x \times N_x}$ is the nonsingular mass matrix. t_0 and t_f are the initial and final time, respectively. We do not impose constraints at the initial time t_0 for those path constraints containing differential or variable states only to avoid infeasible initializations. $\Phi: \mathbb{R}^{N_x} \to \mathbb{R}$ is the objective function, which will be given for each case study later in this section.

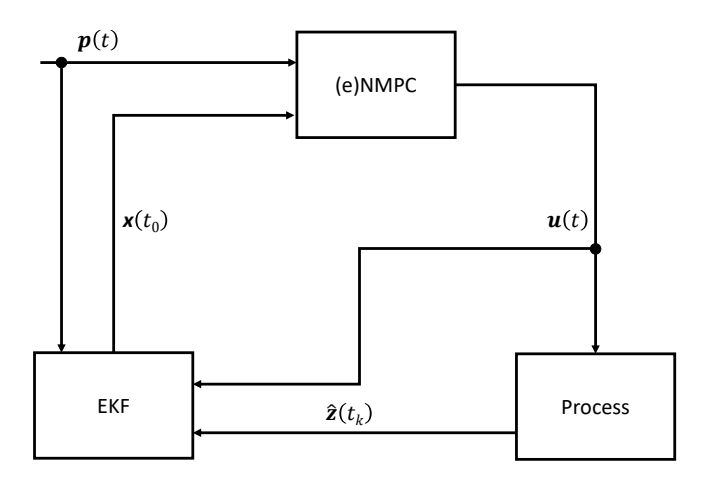


Fig. 2: Control Scheme including NMPC and EKF.

We investigate the application of the TWPM presented in Section 2.2 for NMPC and eNMPC [36]

11 Page 11 of 33 ©A. Caspari et al.

using the control scheme shown in Fig. 2. It consists of an (e)NMPC with the TWPM as an internal model and a state estimator interacting with the process. We apply the scheme in-silico with the process model with the FOM as plant surrogate. The NMPC solves dynamic optimization problems of the form (17) at each sampling time on a moving horizon with a sampling time t_s , and a control horizon $t_h = t_f - t_s$. We use equal prediction and control horizon. The use of the TWPM as controller model leads to plant-model mismatch. We assume to have measurements

$$\boldsymbol{z}(t_k) = \boldsymbol{h}(\boldsymbol{x}(t_k))$$

where $z: \mathcal{T} \to \mathbb{R}^{N_z}$, $h: \mathbb{R}^{N_x} \to \mathbb{R}^{N_z}$, which can be used to estimate the initial state x_0 in each controller sample using a state observer. We use an EKF [37, 38] which also uses the TWPM. We cannot use full state feedback for the TWPM, since (i) the states of the TWPM do not coincide with the states of the FOM and (ii) we aim to illustrate the performenance of the TWPM in a control scheme where a certain selection of measurement are available. We could calculate the states of the TWPM based on the states of the FOM. However, this would be a special type of state estimation tailored to the TWPM. In addition, the goal of the state estimation is rather to find those states of the TWPM for which the TWPM outputs match the measurements at the current iteration as opposed to finding those state values, for which the TWPM states agree with the states of the FOM based on a correlation that we think can be used to match the values of the TWPM states and the FOM states. Therefore, we used an EKF as a generally The weights of the EKF are tuned heuristically. The EKF is initialized applicable state estimator. by repeated EKF runs at the initial plant state in order to guarantee that the plant measurements and the respective TWPM variables are consistent, i.e., the EKF converged to the initial steady-state. The final values of the TWPM states after this initilization procedure are used to initialize the EKF at the beginning of the closed-loop simulations. For comparison, we use both the FOM and the TWPM as 15 controller models. When using the FOM as controller model, we assume ideal control, i.e., no plant-model mismatch and full state feedback, thus no state estimator is required.

$_{\scriptscriptstyle 18}$ 3 Application of the TWPM

We analyze the behavior of the TWPM in-silico in adopen-loop forward simulations, offline dynamic optimizations and use the TWPM as controller model in closed-loop control simulations of an ASU.

First, we present the ASU considered together with the corresponding optimization and control scenarios. Then, we describe the parameter estimation for the TWPM and show the computational results

©A. Caspari et al. 12 Page 12 of 33

from forward open-loop simulations. Thereby we compare the prediction performance of the TWPM with
the original constant holdup wave propagation model of [1]. Finally, we present the computational results
from the offline dynamic optimizations and closed-loop simulations. The results of the offline dynamic
optimizations illustrate the open-loop performance of the TWPM in terms of accuracy and in terms of
CPU time reduction. The closed-loop simulation results show the performance of the TWPM in terms
of accuracy and in terms of CPU time reduction when applied in process control.

We implement the models in Modelica with Dymola and use them as functional mock-up units [39]. We solve the integral in (12) a-priori using symbolic integration. The process unit models are provided in the supplementary material. We use direct single-shooting [40, 41] to solve the dynamic optimization problems of the form (17). However, the propoded reduced model and process operation strategy is not restricted to single-shooting and other approaches for dynamic optimization [42] could also be applied 11 for the solution of the dynamic optimization problems. The computations including the solution of the 12 optimization problems of the form (17) as well as open-loop forward simulations are performed in the 13 dynamic optimization framework DyOS [43] with the DAE integrator NIXE [44] and the NLP solver SNOPT [45]. We use relative and absolute DAE integration tolerances of 10⁻⁶ and NLP feasibility 15 and optimality tolerances of 10^{-5} . The tight tolerances are used in order to facilitate comparability of the computational results without the risk of dealing with numerical artifacts. We use the EKF 17 implementation in FilterPy [46]. We run all calculations on a Microsoft Windows 10 desktop computer with an Intel Core i7-8700 processor running at 3.20 GHz and 16 GB RAM. We average the CPU time of the offline dynamic optimizations over 10 optimizations starting from the same initial condition. The CPU 20 times for the optimizations during the closed-loop simulations are average over all (e)NMPC iterations.

2 3.1 Scenarios for Single Column and ASU Case Studies

Table 1: MVs and constraints for rectification column case study. $\dot{n}_{\rm in}$ column feed stream, $\xi_{\rm LP}$ column splitfactor, $\boldsymbol{x}_{\rm out}$ product purity.

variable	lower bound	upper bound	initial value	\mathbf{type}
$\dot{n}_{\rm in} \; [{\rm mol/s}]$	225	365	300	MV
$\xi_{ m LP}$ [-]	0.48	0.58	0.522	MV
$oldsymbol{x}_{ ext{out}}$ [-]	0.99995	-	-	path constraint

We consider the ASU depicted in Fig. 3, which is used to produce nitrogen from air by cryogenic rectification. The nitrogen product can downstream be fed into a distribution pipeline or can directly be used in subsequent applications, e.g., in steel production. We refer to the textbooks [47, 48] for more detailed information on ASUs and their products. We have used and described the present process and

©A. Caspari et al. 13 Page 13 of 33

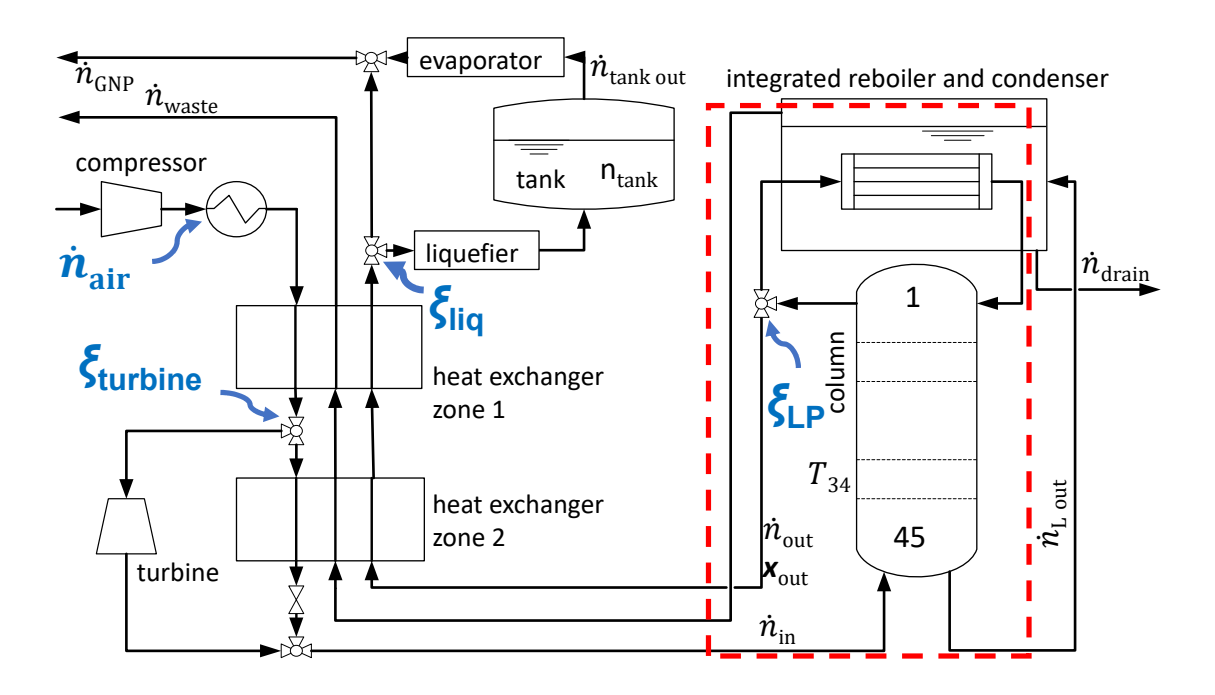
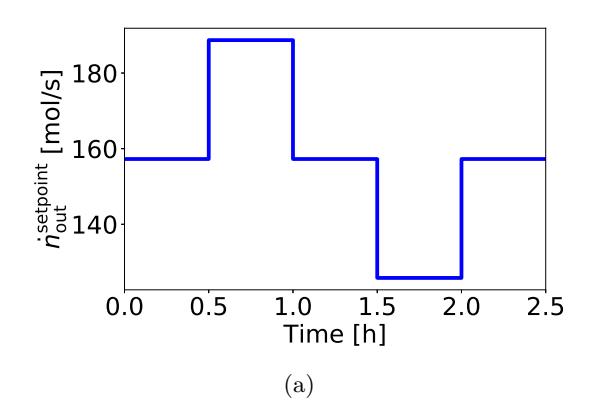


Fig. 3: Flowsheet of single-product ASU. The MVs are indicated in blue and with arrows. The dotted, red rectangle indicates the single column considered as stand alone case study.

- model in recent works [5, 4, 7]. The model equations can be found in [34] and in the supplementary
- $_{2}$ material. Ambient air enters the process. As feed, we consider air as the mixture of 0.78 mol N_{2} /mol air,
- 3 0.21 mol O₂/mol air, and 0.01 mol Ar/mol air. The feed stream is compressed in the main compressor to
- a pressure of 8.5 bar, cooled down in the heat exchanger, partially expanded in the turbine, and enters
- the rectification column at a pressure of 5.5 bar. The distillation column comprises 45 equilibrium stages.
- ⁶ The bottom stream of the distillation column is fed to the reboiler with a pressure of 1.5 bar, which is
- 7 heat integrated with the total condenser. The vapor outlet of the reboiler is a waste stream, the liquid
- outlet a drain stream. The product stream is withdrawn from the column top. It can be liquefied by a
- 9 liquefication cycle and stored in the tank or can directly be withdrawn as product stream. The electricity
- consumers of the process are the compressor and the liquefier. The turbine generates electricity from
- 11 expansion.

To investigate the performance of the TWPM, we consider the distillation column of the ASU separately, before we apply the approach to the entire ASU. The column is shown in Fig. 3, indicated by the red, dashed frame. Cryogenic air at the dew point enters the column at the bottom. The product is withdrawn from the column top. The aim of the single column process is to obtain a product stream

©A. Caspari et al. 14 Page 14 of 33



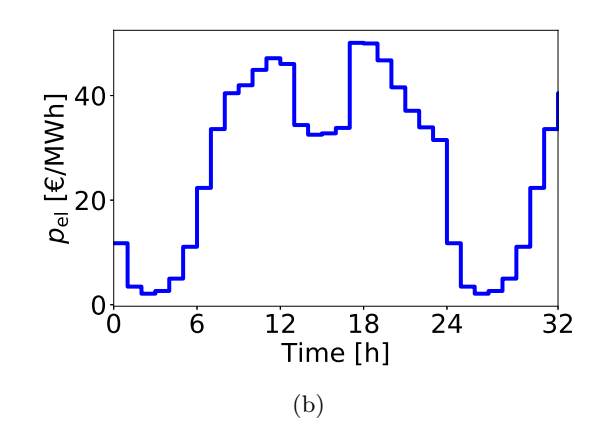


Fig. 4: Scenario profiles for the single column and ASU case studies. (a) Load change profile, i.e., product flowrate setpoint for single distillation column case studies. (b) Electricity price profile for ASU case studies.

Table 2: MVs and constraints for ASU case study. $\dot{n}_{\rm air}$ feed air stream, $\xi_{\rm turbine}$ splitfactor to turbine, $\xi_{\rm LP}$ column splitfactor, $\xi_{\rm liq}$ splitfactor to product stream, $x_{\rm GNP}^{\rm N_2}$ product purity at column top, $\dot{n}_{\rm tank,out}$ tank outlet stream, $\dot{n}_{\rm drain}$ reboiler outlet liquid stream, $n_{\rm tank}$ storage tank holdup. The MVs are initialized with a constant profile.

variable	lower bound	upper bound	initial value	type
$\dot{n}_{\rm air} \; [{ m mol/s}]$	225	365	320	MV
ξ_{turbine} [-]	0.75	0.95	0.85	MV
$\xi_{ m LP}$ [-]	0.50	0.54	0.52	MV
$\xi_{ m liq}$ [-]	0	1	1	MV
$x_{\text{GNP}}^{N_2}$ [-]	0.99995	-	-	path constraint
$\dot{n}_{\rm tank,out} \; [\rm mol/s]$	0	20	-	path constraint
$\dot{n}_{\mathrm{drain}} \; [\mathrm{mol/s}]$	1	10	-	path constraint
$n_{\rm tank} \ [10^7 \ {\rm mol}]$	1.330	-	-	terminal constraint

with a specific minimum nitrogen purity. The MVs and the constraint are summarized in Tab. 1. We analyze the use of the TWPM for a load change, i.e, tracking of product flow setpoints and minimize the following objective

$$\Phi_1 = \int_{t_0}^{t_f} \left(\dot{n}_{\text{out}}(t) - \dot{n}_{\text{out}}^{\text{setpoint}}(t) \right)^2 dt,$$

- i.e., we aim to minimize the deviation of the outlet stream $\dot{n}_{\rm out}$ from a given setpoint $\dot{n}_{\rm out}^{\rm setpoint}$ subject
- to the product purity constraint. Such a load change can occur frequently within a day, e.g., when the
- nitrogen demand of the downstream process changes. We apply the setpoint profile from Fig. 4a and
- assume the setpoint profile to be known by the NMPC during the closed-loop simulation, i.e., the NMPC
- 5 makes exact setpoint profile predictions. The offline dynamic optimization results of the distillation
- 6 column load change, i.e., product flowrate setpoint tracking case study are shown in Section 3.4.1 and
- ⁷ the closed-loop results in Section 3.5.1. Both offline dynamic optimization and closed-loop case study
- ⁸ use the same objective function and constraints. The FOM of the plant surrogate comprises 45 stages

©A. Caspari et al. 15 Page 15 of 33

- and uses a hydraulic factor of $k_d = 0.5 \text{ s}^{-1}$. We give the parameter values for the TWPM in Section 3.2.
- The process model with the FOM comprises 136 differential states and about 2450 algebraic states. The
- process model with the TWPM comprises 3 differential states and 368 algebraic states.

In the ASU case studies, we optimize the process operation of the entire ASU with respect to its operating cost by adjusting the instantaneous production rate to the cost of electricity, which is a realization of demand side management. For further information on demand side management, we refer to [49, 50, 7]. The flexible operation promises economic advantages over a stationary process operation. Thus, we minimize the economic objective

$$\Phi_2 = \int_{t_0}^{t_f} (p_{\rm el}(t) \cdot P_{\rm total}(t)) \, \mathrm{d}t,$$

where $p_{\rm el}: \mathcal{T} \to \mathbb{R}$ is the electricity price and $P_{\rm total}: \mathcal{T} \to \mathbb{R}$ is the total power usage of the process. We use the electricity price profile from Fig. 4b, which is taken from historic electricity price data of the German day ahead market and assume the electricity price to be known by the eNMPC during the closed-loop simulation, i.e., the eNMPC makes exact electricity price predictions. The process power consumption is calculated with

$$P_{\text{total}}(t) = P_{\text{compressor}}(t) + P_{\text{liquefier}}(t) - P_{\text{turbine}}(t),$$

where $P_{\text{compressor}}: \mathcal{T} \to \mathbb{R}$ and $P_{\text{liquefier}}: \mathcal{T} \to \mathbb{R}$ are the power usage of compressor and liquefier, and $P_{\text{turbine}}: \mathcal{T} \to \mathbb{R}$ is the power generated by the turbine. We calculated the power demand of the compressor by

$$P_{\text{compressor}}(t) = \dot{n}_{c}(t) \cdot (h_{c,\text{out,isen}}(t) - h_{c,\text{in}}(t)) / \eta_{\text{isen.c}},$$

where $\dot{n}_c \in \mathbb{R}$ is the molar flowrate of the feed stream, $h_{c,in} \in \mathbb{R}$ the enthalpy of the feed stream, $h_{c,out,isen} \in \mathbb{R}$ the outlet enthalpy assuming an isentropic compression, and $\eta_{isen,c} \in \mathbb{R}$ the isentropic efficiency. Similarly, we use the following equation for the turbine power supply

$$P_{\text{turbine}}(t) = \dot{n}_{\text{t}}(t) \cdot \left(h_{\text{t,in}}(t) - h_{\text{t,out,isen}}(t) \right) \cdot \eta_{\text{isen.t}},$$

where $\dot{n}_c \in \mathbb{R}$ is the molar flowrate in the turbine, $h_{t,in} \in \mathbb{R}$ the enthalpy of the feed stream, $h_{t,out,isen} \in \mathbb{R}$ the outlet enthalpy assuming an isentropic expansion, and $\eta_{isen,t} \in \mathbb{R}$ the isentropic efficiency. We assume $\eta_{isen,t} = \eta_{isen,c} = 0.8$. We refer to [51] for further details about the turbine and compressor models. The

©A. Caspari et al. 16 Page 16 of 33

power demand of the liquefier is calculated by

$$P_{\text{liquefier}}(t) = \dot{n}_{\text{liq}}(t) \cdot \left(T_{\text{liq,in}} \cdot \left(s_{\text{liq,in}}(t) - s_{\text{liq,out}}(t) \right) - \left(h_{\text{liq,in}}(t) - h_{\text{liq,out}}(t) \right) \right) / \eta_{\text{liq,out}}(t)$$

where $\dot{n}_{\text{liq}} \in \mathbb{R}$ is the feed flowrate to the liquefier, $s_{\text{liq,in}} \in \mathbb{R}$ and $s_{\text{liq,out}} \in \mathbb{R}$ the enthalpies of the feed

stream and leaving stream, and $h_{\text{liq,in}} \in \mathbb{R}$ and $h_{\text{liq,out}} \in \mathbb{R}$ the enthalpies of the feed stream and leaving stream. $\eta_{\text{liq}} \in \mathbb{R}$ is the liquefier efficiency, for which we assume $\eta_{\text{liq}} = 0.4$. We further assume that the leaving stream of the liquefier is saturated liquid at a pressure of 1.2 bar. We refer to [34] for further details about the liquefier model. The initial guess and bounds on MVs and constraints are summarized in Tab. 2. The initial values of the MVs result in a feasible steady-state. We selected those variables as MVs which can be manipulated in a real process. The product purity constraint corresponds to common technical product specifications, e.g., [47]. We select the constraints on $\dot{n}_{\rm tank,out}$ to prevent a negative tank withdrawal stream and to allow maximum about 10% of the nominal product stream to be provided from tank withdrawal. We 10 use the constraints on \dot{n}_{drain} to guarantee certain reboiler holdups (the drain stream is calculated using a 11 linear hydraulic correlation with the holdup) and maximum drain streams. The lower bound of the tank 12 holdup at the final time (terminal constraint) corresponds to the initial tank holdup. The MV bounds 13 have been selected around the nominal, feasible steady-state values. The ranges have been chosen so that the process can be operated with a certain level of flexibility. The ranges are given by the process 15 design for the several pre-defined operating cases. The FOM and TWPM are the same as in the single column case studies explained above. The process model with the FOM as column model comprises of 149 differential states and 2833 algebraic states. The process model with the TWPM as column model comprises of 26 differential states and 912 algebraic variables. The offline dynamic optimization results 19 of ASU case study are shown in Section 3.4.2. The closed-loop results are shown in Section 3.5.2. Both 20 offline dynamic optimization and closed-loop case study use the same objective function and constraints.

© A. Caspari et al. 17 Page 17 of 33

3.2 Parameter Estimation and Approximation Quality of the TWPM

Table 3: Estimated parameter values for the TWPM.

parameter	parameter value		
B [-]	24.0920		
α^{N_2} [-]	3.2019		
α^{Ar} [-]	1.3162		
k_d [1/s]	0.0103728		

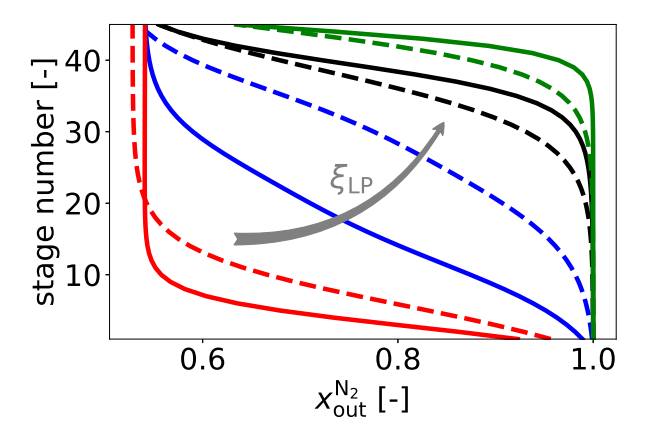


Fig. 5: Steady-state nitrogen concentration profiles of the TWPM (dashed lines) and the FOM (solid lines) over stages for different column split factors. Red, $\xi = 0.48$. Blue, $\xi = 0.51$. Black, $\xi = 0.53$. Green, $\xi = 0.63$.

We explain the parameter estimation for the TWPM and analyze the steady-state accuracy of the TWPM used in the case studies. Therefore, we consider the single ASU column case as described in Section 3.1. The parameter estimation is based on steady-state data of the FOM, which is provided in the supplementary material. It is similar to the models used, e.g., in [33, 34, 52]. The transient accuracy is shown later in the case studies in the sections 3.4 and 3.5. The values of the TWPM parameters B, α_i , and k_d are estimated based on the steady-state concentration profiles and the molar holdup of the FOM. They could also be estimated based on plant measurements. The estimation based on real measurements might be more complicated since information on the full concentration profile inside the column could not be available. However, similar parameter estimation problems could be used taking into account only the input-output data of the column or concentration and temperature measurements from selected positions inside the column. For the estimation of B and α_i , we solve a steady-state optimization problem using a least-square error formulation. We provide the optimization problem formulation in the supplementary material. The relative volatilities are considered as parameters to be estimated, since we use constant

©A. Caspari et al. 18 Page 18 of 33

21

22

values for the overall column. We obtain satisfactory results in the open- and closed-loop case studies using the model with the estimated relative volatilities, which we present in Section 3. Alternatively, the volatilities could be calculated based on an average temperature and pressure in the column. However, this would complicate the model. The parameter k_d is directly calculated based on the total molar holdup and the liquid outlet stream of the FOM using: $k_d = \dot{n}_{\rm L,out}/n_{\rm total}$. We use $\xi = 0.53$ and $\dot{n}_{\rm in} = 300$ mol/s as operating point for the parameter estimation. The estimated parameters are given in Table 3. We also determined the mean values of the relative volatilities over the column height at the nominal operating point for comparison and obtained $\bar{\alpha}^{\rm N_2} = 3.03$ and $\bar{\alpha}^{\rm Ar} = 1.29$, which are close to the values in Table 3. We could thus take these mean values and perform the parameter estimation just for B as well.

Fig. 5 shows the profiles for different values of the splitfactor ξ_{LP} for the FOM and the TWPM. Only the splitfactor is varied. The column feed is kept constant. Note that the TWPM uses idealized 11 assumptions, e.g., constant relative volatilities α_i and ideal thermodynamic behavior, which are violated 12 in our case. Nevertheless, the TWPM predicts the molar fraction profiles of a FOM qualitatively correct. 13 The mean relative error over all profiles is 4% with a standard deviation of 12% and a maximum error of 14 50%. Despite these deviations in the column, the mole fractions of the exiting streams are predicted more 15 accurately. In the case studies of the sections 3.4 and 3.5, we show that the model can be successfully applied for offline dynamic optimization and closed-loop control simulations. This is not obvious since the 17 TWPM profiles in the column affect the state estimation, which uses a single temperature measurements of the column to estimate the states of the TWPM in the closed-loop simulations.

3.3 TWPM versus Constant Holdup Wave Propagation Model

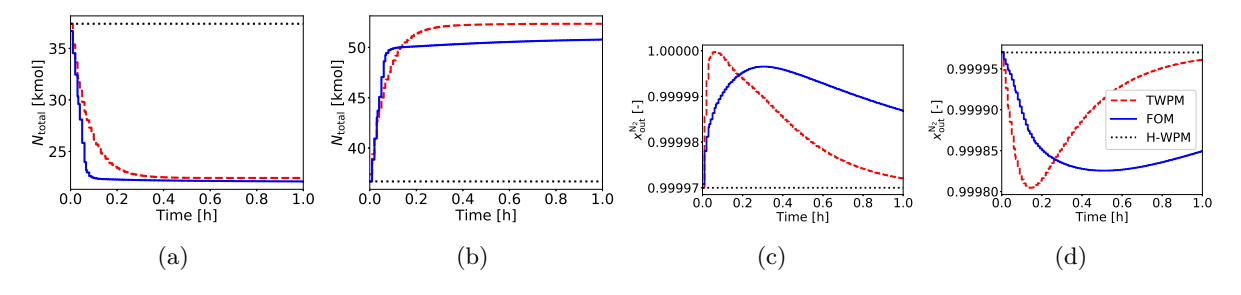


Fig. 6: Molar column holdups and Nitrogen molar fractions of TWPM, FOM, and H-WPM during load changes. (a)/(b) Holdup at load change during -40 %/+40 % feed stream. (c)/(d) Nitrogen mole fraction at load change during -40 %/+40 % feed stream.

We compare the prediction performance of the TWPM with the performance of the constant holdup wave propagation model proposed by [1]. Therefore, we perform open-loop forward simulations of the single column with a step in the feed stream of +40% and -40%. We keep the other MV ξ_{LP} as well as

©A. Caspari et al. 19 Page 19 of 33

11

15

- the feed conditions constant during the simulations. The profiles are shown in Fig. 6. We see that the
- holdup of the FOM varies during these load changes and achieves a new level. Further, the TWPM is
- able to predict the total column holdup during the load changes with satisfactory accuracy. The TWPM
- achieves the same steady-state. In contrast, the holdup is assumed to be constant by the reduced model
- proposed by [1], indicated as H-WPM. The constant column holdup model of Kienle [21] is not able to
- represent transient behavior for such load changes, whereas the TWPM is.
- In [21], constant volume is assumed for each stage, which requires the volume calculation for every
- column stage and lead thus to higher computational demand for optimization. In addition, the volume
- calculation on every stage would lead to the reduced model scaling with the number of column stages.
- In contrast, the size of TWPM and H-WPM are independent of the column size.
- variations during the load changes qualitatively correct and quantitatively satisfactory. In contrast, the 12 product purity of the H-WPM is constant during the load changes. In the turn-up load change, the 13

We see that the product purity varies during load changes. The TWPM is able to predict the purity

- product purity decreases, so that the splitfactor would need to be adjusted in order to meet possible
- purity constraints. Since the H-WPM predicts a constant product purity, a model-based controller with
- this model would not be able to effectively counteract the purity decrease. Although we do not get the
- same quantitative behavior, we think the suitability of the TWPM as controller model is justified.

Application of TWPM in Dynamic Offline Optimization 3.4 18

- We present the results of the dynamic offline optimizations. Every optimization is performed using the
- FOM and the TWPM. For comparison, the MV profiles resulting from the optimization with the reduced
- model are used in a forward simulation of the FOM.

Dynamic Offline Optimization of Distillation Column

- We optimize the single distillation column over a time horizon of 2.5 h, i.e., $t_0 = 0$ and $t_f = 9000$ s, and 23
- use piecewise constant MV profiles with a discretization of 2 min. The path constraints are evaluated on 24
- the same grid. We denote the trajectories resulting from the optimization with the FOM as offline-FOM 25
- and those from the optimization with the reduced model as offline-TWPM. 26
- The results are shown in Fig. 7. We see that both MV and state profiles of the TWPM and the FOM 27
- are similar. There are only small deviations in the MV profiles (Figs. 7a and 7b). The product stream is
- tracked to its setpoint successfully (Fig. 7c) and the product purity constraint is satisfied (Fig. 7d). The
- similar profiles indicate correct physical behavior of the TWPM; it captures well the dynamic behavior

20 Page 20 of 33 ©A. Caspari et al.

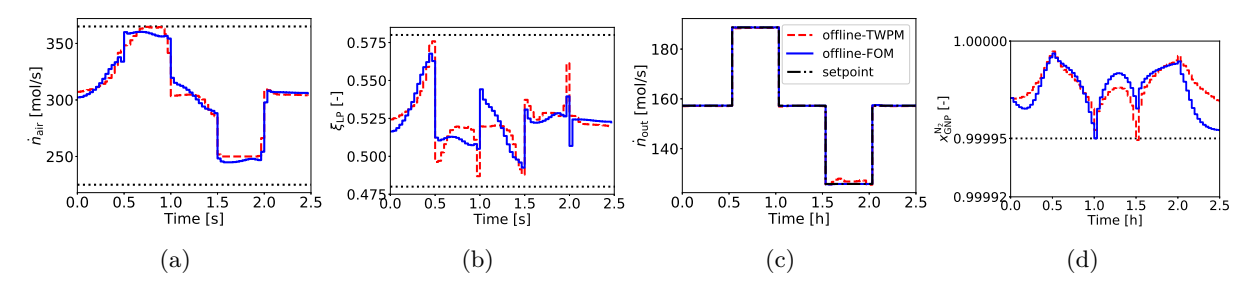


Fig. 7: MV and state variable profiles from offline optimization with FOM and TWPM. The state profiles result from FOM by simulation with the MV profiles resulting from the optimization with FOM and TWPM. The MV profiles are piecewise constantly discretized with 2 minutes intervals. Bounds black dotted. (a) Air feed stream (MV). The mean deviation between the two profiles is 1.4%. (b) Column splitfactor (MV). The mean deviation between the two profiles is 1.3%. (c) Column product stream (state variable). (d) Column product concentration (state variable).

of the FOM.

- The CPU time for the optimization of the TWPM is reduced significantly compared to the time for
- the optimization with the FOM (Tab. 4). Thus, the TWPM can be used as an efficient reduced model
- 4 for optimization.
- In Appendix A, we show results of the same case study with the model of Kienle [1] assuming constant
- 6 column holdup instead of the TWPM. The TWPM performs slightly better than the constant holdup
- 7 wave propagation model in terms of accuracy, although the constant holdup model cannot represent a
- 8 transient column behavior.

9 3.4.2 Offline Dynamic Optimization of ASU

- We perform an offline dynamic optimization for the ASU over a time horizon of 1 d, i.e., $t_0 = 0$ and $t_f = 86400$ s. We use piecewise constant MV profiles with a discretization of 2 h. The path constraints are evaluated every 24 min. All trajectories shown result from the simulation of the FOM with the MVs from the optimization with the FOM and the TWPM, respectively. We denote the former as offline-ASU-FOM and the latter as offline-ASU-TWPM.
- Fig. 8 shows the MVs and selected state variables. The MV profiles are similar for both the optimization with the FOM and with the TWPM. This translates into similar state profiles. There is a slight offset of about 10⁻⁵ in the molar fraction of nitrogen in the GNP stream (Fig. 8g). This offset, however, is positive so that the constraint is not violated. Both the optimization using the FOM and the TWPM lead to satisfaction of the path constraints (Figs. 8e-8g) and the terminal constraint (Fig. 8h).
- The CPU time for the optimization with the TWPM is significantly reduced compared to the time for the optimization with the FOM. We achieve a speed-up factor of 32. Thus, the TWPM can efficiently

©A. Caspari et al. 21 Page 21 of 33

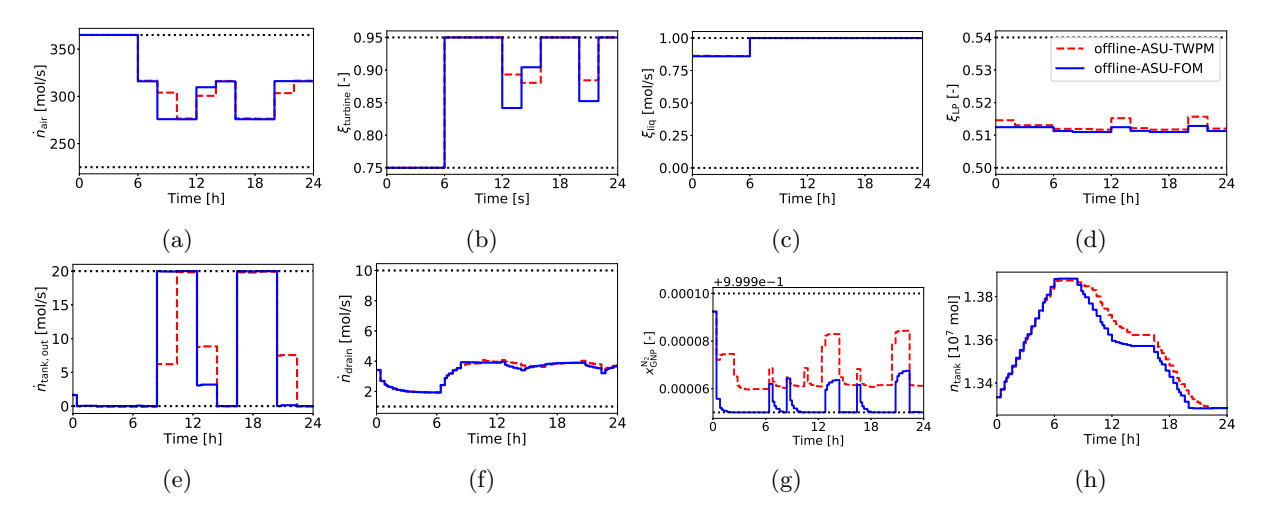


Fig. 8: MV profiles and selected state profiles from offline optimization of ASU. Bounds black dotted. (a) Feed air flowrate (MV). Mean relative deviation 1%. (b) Splitfactor turbine (MV). Mean relative deviation 1%. (c) Splitfactor liquefier (MV). Mean relative deviation 0.1%. (d) Splitfactor column (MV). Mean relative deviation 0.2%. (e) Tank outlet stream flowrate (state variable). (f) Reboiler drain stream flowrate (state variable). (g) Molar fraction of nitrogen in GNP stream (state variable). (h) Tank holdup (state variable).

be used as a reduced model within a flowsheet for optimization.

2 3.5 Application of the TWPM in Model-Based Control

- We present in-silico closed-loop case studies in this section. The first is a load change, i.e., product flow
- 4 setpoint tracking of the single distillation column using an NMPC. The second is the flexible operation of
- 5 an ASU under fluctuating electricity prices using an eNMPC. The shown results are always the trajectories
- 6 of the plant surrogates, i.e., the process models with the FOM.

7 3.5.1 Tracking of Load Changes of a Distillation Column Using NMPC

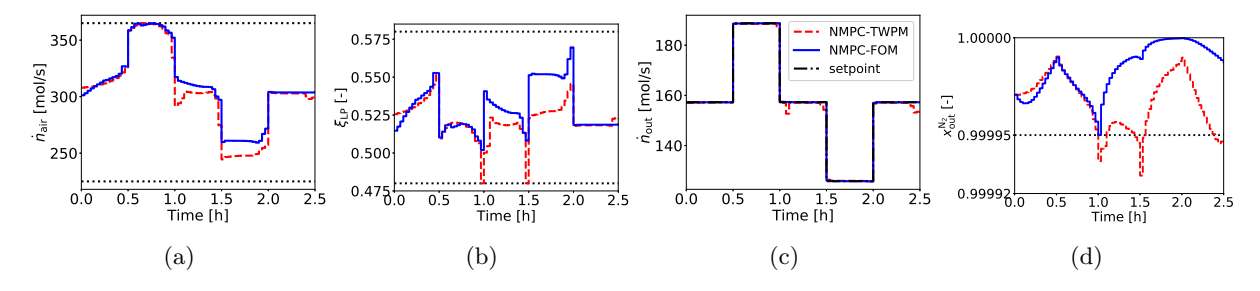


Fig. 9: Closed-loop control simulation results of distillation column for GNP load change with full model and reduced model. Bounds black dotted. (a) Air flow (MV). Average deviation between full model and reduced model profile 2.1%. (b) Splitfactor (MV). Average deviation between full model and reduced model profile 1.7%. (c) GNP flow (state variable). (d) GNP concentration (state variable).

©A. Caspari et al. 22 Page 22 of 33

12

13

14

15

The measured variables for the EKF are the product concentration x_{out} , the temperature T_{34} on column stage 34, and the liquid outlet stream \dot{n}_{out} . We denote the profiles with FOM as the controller model as NMPC-FOM and those with TWPM as NMPC-TWPM. We use a control horizon of $t_h=1$ h and a sampling time of $t_s=2$ min.

Fig. 9 shows the process profiles as results of the closed-loop control simulation. We see only small deviations in the MVs between NMPC-TWPM and NMPC-FOM (Figs. 9a and 9b). The product stream setpoint profile is successfully tracked by both NMPC-FOM and NMPC-TWPM (Fig. 9b). There are only minor deviations from the setpoint profiles. Remember that the NMPC-TWPM does not use state feedback but state estimates from the EKF. Thus, both plant-model mismatch and deviations due to state estimation may be the roots of the small deviations between the profiles. The purity constraint is satisfied most of the time (Fig. 9d).

The computational demand for the solution of the optimization problems of the NMPC-TWPM is significantly less than for the NMPC-FOM (Tab. 4). We have a speed-up factor of about 190. The NMPC-TWPM is real-time applicable with CPU time of less then 2% of the sampling time in average and maximum 22% of the sampling time. In contrast, the NMPC-FOM does not appear to be real-time applicable; the mean CPU time for the dynamic optimization is higher than the sampling time. The computational time used by the EKF is negligible as it is significantly lower than that for the NMPC.

3.5.2 Flexible Operation of ASU Using eNMPC

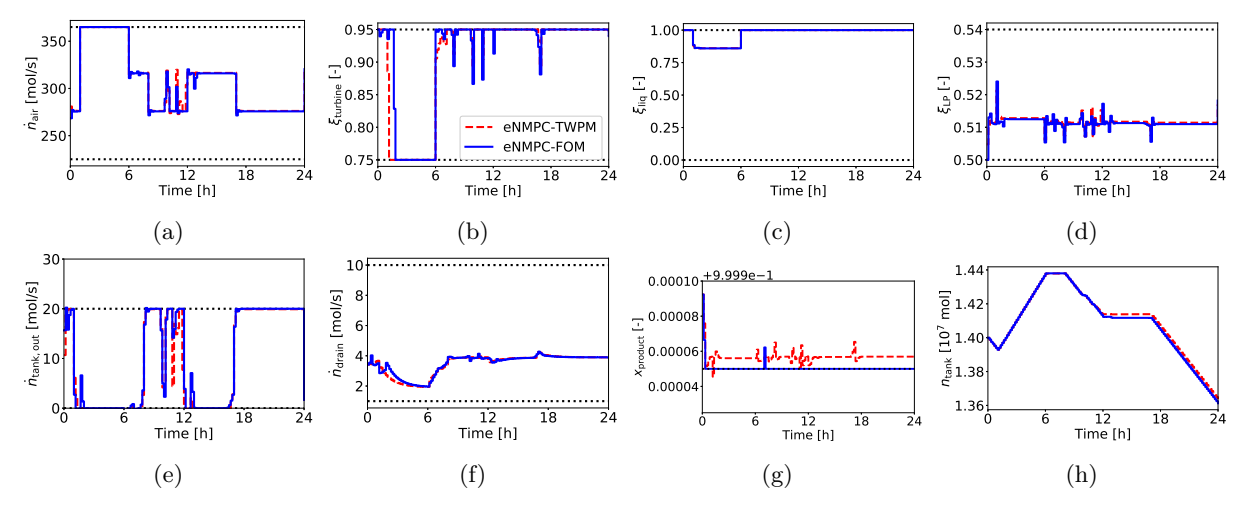


Fig. 10: MV profiles and selected state profiles from closed-loop optimization of ASU. Bounds black dotted. (a) Air feed stream (MV). Mean relative deviation 0.4%. (b) Turbine splitfactor (MV). Mean relative deviation 0.8%. (c) Liquefier splitfactor (MV). Mean relative deviation 0.01%. (d) Column splitfactor (MV). Mean relative deviation 0.1%. (e) Tank outlet stream (state variable). (f) Reboiler drain stream (state variable). (g) Product purity (state variable). (h) Tank holdup (state variable).

©A. Caspari et al. 23 Page 23 of 33

For the case considering the flexible operation of the ASU using eNMPC, we denote the profiles resulting from the eNMPC with FOM as controller model as eNMPC-FOM and those with TWPM as controller model as eNMPC-TWPM.

We use full state feedback for the heat exchangers, the reboiler, and the storage tank. We do not assume full state feedback for the column for the eNMPC-TWPM. The initial state for the TWPM is estimated using an EKF based on measurements of the outlet concentration of the FOM $y_{\text{out}}^{N_2}$, the temperature T_{34} on stage 34 of the column, and the liquid outlet flowrate $\dot{n}_{\text{L,out}}$. We obtain the temperature on the 34. stage by performing an enthalpy calculation based on the molar fraction from the wave propagation model at this stage. For the eNMPC, we use a sampling time of 10 min and a control horizon of 8 h. The MVs are discretized with 10 min intervals for the first hour and with 1 h intervals for the remaining control horizon. We perform the case study over a time horizon of one day.

The eNMPC-FOM achieves operation cost of 1890 € after one day of operation, whereas the eNMPC-12 TWPM achieves $1896 \in$, i.e., the difference in the economic performance is about 0.3%. The resulting 13 trajectories are shown in Fig. 10. We see that the MV profiles of eNMPC-FOM and eNMPC-TWPM 14 are close to each other. The mean relative deviation is less than 1% for all profiles. We further see 15 that the eNMPC achieves an economically intuitive process operation: the feed air stream and liquefier stream/tank feed stream are increased, when the electricity price is low, and decreased otherwise (Figs. 17 10a and 10c). The highly accurate MV profiles translate in nearly identical state profiles. Both eNMPC-FOM and eNMPC-TWPM achieve constraint satisfaction (Figs. 10e, 10f, and 10g). Product is filled into the tank, when the electricity price is low, and is withdrawn from the tank otherwise (Figs. 10e and 10h). 20 An offset in the nitrogen purity, that has been observed earlier (Sec. 3.4.2), can again be observed in this 21 case study (Fig. 10g). However, the offset does not lead to constraint violation and could be eliminated 22 using offset-free model predictive control methods [53]. Both MV and state profiles are similar to the 23 offline dynamic optimization profiles presented in Sec. 3.4.2. The eNMPC-TWPM achieves even higher 24 accuracy with respect to the eNMP-FOM compared to the profiles of the offline dynamic optimization (cf. Figs. 8 and 10). This underlines the suitability of the reduced model as controller model in the process control strategy described in Section 2.3. The feature that eNMPC achieves similar MV profiles compared to the corresponding offline optimization, even when a sub-optimal method is applied, has already been pointed out in the literature [11, 7]. 29

Tab. 4 gives the CPU times for eNMPC-FOM and eNMPC-TWPM. The eNMPC-TWPM optimizations are faster than the eNMPC-FOM optimizations by more than 95%, i.e., we have a speed-up factor of more than 20. In addition, the eNMPC-FOM optimizations take in average nearly as long as the

©A. Caspari et al. 24 Page 24 of 33

- 1 eNMPC sampling time and the maximum time is much longer than the sampling time. Thus, real-time
- applicability cannot be guaranteed for the eNMPC-FOM. The eNMPC-TWPM optimizations are in av-
- erage significantly lower than the sampling time and even the maximum time is only 20% of the sampling
- 4 time indicating real-time applicability. The time for the EKF is negligible. The eNMPC-TWPM is thus
- applicable in real-time with the optimization problems solved until local convergence, i.e., not only with
- a suboptimal fast-update method [7] as in [4] with compartment models.

Table 4: Summary of CPU times for all case studies. The offline optimizations are executed 10 times starting from the same initial conditions and average computational times are reported. The times for the closed-loop optimizations are averaged over all NMPC/eNMPC iterations to get the mean. The maximum value is obtained by taking the maximum CPU time over all (e)NMPC samples. The CPU time savings are in the order of a factor of 100 with acceptable accuracy as shown in the figures.

	\mathbf{TWPM}	\mathbf{FOM}	\emptyset CPU time reduction
offline column	3.1 s	1190.3 s	99.7%
offline ASU	$52.0 \mathrm{\ s}$	$1644.7 \; \mathrm{s}$	96.8%
closed-loop column mean/max	1.7/3.9 s	$319.8/747.0 \mathrm{\ s}$	99.5/99.5%
closed-loop ASU mean/max	23.0/124.0 s	474.48/8631.8 s	95.2/99%

₇ 4 Conclusions

- We propose a reduced model for multicomponent distillation columns based on nonlinear wave propa-
- 9 gation and use it for offline dynamic optimization and nonlinear model predictive control. We thereby
- combine the ideas of compartment modeling and nonlinear wave propagation. The reduced model is able
- 11 to adequately represent steady-state and transient behavior, as is required in particular to capture load
- 12 change behavior. The proposed reduced model has the advantage that only a few parameters have to be
- estimated which can be fitted to steady-state data from a more detailed model or from a real plant. This
- 14 facilitates the model's practical application and enables usage in those usual situations where steady-state
- data from plant operation or process design is available only.
- The proposed model can, thus, be used as controller model in nonlinear model-based control not only
- for disturbance rejection, as has been done in previous works, but also for flexible operation, as we show
- in this article.
- We show that the TWPM leads to physical behavior during column load changes, whereas existing

©A. Caspari et al. 25 Page 25 of 33

reduced models based on wave propagation admit nonphysical behavior. We perform offline dynamic optimization and closed-loop control case studies for an ASU. To study the impact of the TWPM on a single column, we focus on the distillation column of the ASU first before we consider the entire process. We compare the performance and accuracy of the TWPM with those of the FOM. In the closed-loop control case studies we compare with an ideal model predictive controller, i.e., without plant-model mismatch and with full state feedback. The reduced model achieves significant CPU time reductions of more than 95% and up to more than 99% for dynamic optimization in all presented case-studies. Accordingly, the TWPM achieves higher computational saving than the reduced column models reported in literature. The TWPM leads to a smaller DAE compared to the FOM. In contrast to the FOM, the size of the DAE of the TWPM is independent of the column size. Thus, the savings can be even higher for larger columns than those considered in this work, as occur, e.g., in ASUs with argon columns 11 [10, 54]. The mean error between the control variable profiles of the TWPM and FOM are less than 2 12 % in the offline dynamic optimizations and the closed-loop simulations. This illustrates that the reduced 13 model we propose can efficiently be used for optimization and control. Using the proposed TWPM as 14 controller model leads to systems applicable in real-time, even if the controller optimization problems are 15 solved until local convergence. In contrast to our previous work [11], we are not restricted to suboptimal fast-update methods. The maximum time for the solution of a dynamic optimization problem in the 17 closed-loop control case studies with the TWPM is about 20% of the controller sampling time. The controller with the TWPM requires in average less than 2% of the sampling time for the optimizations. The optimizations with the FOM is hardly applicable in real-time in the closed-loop. In contrast, the 20 TWPM enables real-time applicability in the closed-loop application, even when the maximum times 21 for the solution of the optimization problems is considered. As the wave propagation model is derived 22 for ideal thermodynamic mixtures, the reduced model we proposed cannot be expected in general to 23 perform well for highly non-ideal mixtures. However, we demonstrated the model can successfully applied 24 to control a system which does not exhibit ideal thermodynamic behavior.

We observe a small positive offset in the state profiles of the product purity. However, it leads to more conservative control profiles and could in addition be reduced using offset-free NMPC methods [53, 55] or modifier adaptation [56], which is left for future work. This directs the focus also to a systematic approach for the rejection of other persistent disturbances other than plant-model mismatch. An interesting future task is also the application of nonlinear wave propagation models for more complex ASU topologies, e.g.,, a multi-product ASU with a double column [57], with an integrated liquefication cycle [58, 32], or argon columns [10, 54]. As we showed the real-time capable application of NMPC based on the

©A. Caspari et al. 26 Page 26 of 33

- proposed reduced model to an entire ASU in-silico, we think the application to real plants is a promising
- ² future work. The control of other separation processes, e.g., reactive distillation or chromatography using
- nonlinear wave propagation [59] is also of future interest. One key idea of our work is to combine the
- 4 compartment approach and the wave propagation approach to describe the concentration profile within
- one compartment. An interesting task for future research is to study whether other reduced models
- 6 can be applied to describe the concentration profile in a compartment or whether the nonlinear wave
- 7 propagation models can be further extended to include transient effects and applied in optimization and
- 8 control similar to the model in [28].
- Acknowledgement: The authors gratefully acknowledge the financial support of the Kopernikus project
- SynErgie by the Federal Ministry of Education and Research (BMBF) and the project supervision by the
- project management organization Projektträger Jülich (PtJ). We thank Prof. Wolfgang Marquardt for
- 12 fruitful discussions on existing literature and the use of wave propagation models, and Johannes Faust
- and Jan Schulze from AVT for proof reading.

14 References

- [1] A. Kienle, "Low-order dynamic models for ideal multicomponent distillation processes using nonlinear wave propagation theory," *Chemical Engineering Science*, vol. 55, no. 10, pp. 1817–1828, 2000.
- [2] W. Marquardt, "Nonlinear model reduction for optimization based control of transient chemical processes," Chemical Process Control VI. Tucson. Arizona, no. 326, pp. 12–42, 2001.
- [3] M. A. Henson, "Nonlinear model predictive control: current status and future directions," Computers

 & Chemical Engineering, vol. 23, no. 2, pp. 187–202, 1998.
- [4] P. Schäfer, A. Caspari, A. Mhamdi, and A. Mitsos, "Economic nonlinear model predictive control using hybrid mechanistic data-driven models for optimal operation in real-time electricity markets:

 In-silico application to air separation processes," *Journal of Process Control*, vol. 84, pp. 171–181, dec 2019.
- [5] A. Caspari, C. Tsay, A. Mhamdi, M. Baldea, and A. Mitsos, "The integration of scheduling and
 control: Top-down vs. bottom-up," under review, 2019.
- [6] A. U. Raghunathan, M. S. Diaz, and L. T. Biegler, "An MPEC formulation for dynamic optimization
 of distillation operations," Comput. Chem. Eng., vol. 28, no. 10, pp. 2037–2052, 2004.

©A. Caspari et al. 27 Page 27 of 33

- 1 [7] A. Caspari, J. M. Faust, P. Schäfer, A. Mhamdi, and A. Mitsos, "Economic nonlinear model pre-
- dictive control for flexible operation of air separation units," IFAC-PapersOnLine, vol. 51, no. 20,
- рр. 295–300, 2018.
- [8] Y. S. Cho and B. Joseph, "Reduced-order steady-state and dynamic models for separation processes.
- part i. development of the model reduction procedure," AIChE Journal, vol. 29, no. 2, pp. 261–269,
- 6 1983.
- ⁷ [9] Y. S. Cho and B. Joseph, "Reduced-order steady-state and dynamic models for separation pro-
- cesses. part II. application to nonlinear multicomponent systems," AIChE Journal, vol. 29, no. 2,
- pp. 270–276, 1983.
- 10 [10] Y. Cao, C. L. E. Swartz, J. Flores-Cerrillo, and J. Ma, "Dynamic modeling and collocation-based
- model reduction of cryogenic air separation units," AIChE Journal, vol. 62, no. 5, pp. 1602–1615,
- 2016.
- 13 [11] P. Schäfer, A. Caspari, K. Kleinhans, A. Mhamdi, and A. Mitsos, "Reduced dynamic modeling
- approach for rectification columns based on compartmentalization and artificial neural networks,"
- 15 AIChE Journal, vol. 65, no. 5, p. e16568, 2019.
- 16 [12] A. Benallou, D. E. Seborg, and D. A. Mellichamp, "Dyanmic compartmental models for separation
- processes," AIChE Journal, vol. 32, no. 7, pp. 1067–1078, 1986.
- 18 [13] S. Bian, S. Khowinij, M. A. Henson, P. Belanger, and L. Megan, "Compartmental modeling of high
- purity air separation columns," Computers & Chemical Engineering, vol. 29, no. 10, pp. 2096–2109,
- 2005.
- 21 [14] E. Gilles and B. Retzbach, "Reduced models and control of distillation columns with sharp temper-
- ature profiles," in 1980 19th IEEE Conference on Decision and Control including the Symposium on
- 23 Adaptive Processes, IEEE, 1980.
- ²⁴ [15] E. Gilles and B. Retzbach, "Reduced models and control of distillation columns with sharp temper-
- ature profiles," *IEEE Transactions on Automatic Control*, vol. 28, no. 5, pp. 628–630, 1983.
- ²⁶ [16] W. Marquardt, "Wellenausbreitung in verfahrenstechnischen prozessen," Chemie Ingenieur Technik,
- vol. 61, no. 5, pp. 362–377, 1989.
- ²⁸ [17] W. Marquardt, "Traveling waves in chemical process," International chemical engineering, vol. 30,
- no. 4, pp. 585–606, 1990.
 - ©A. Caspari et al. 28 Page 28 of 33

- [18] Y. Cao, C. L. E. Swartz, and J. Flores-Cerrillo, "Optimal dynamic operation of a high-purity air
- separation plant under varying market conditions," Industrial & Engineering Chemistry Research,
- vol. 55, no. 37, pp. 9956–9970, 2016.
- [19] W. Marquardt, "Nonlinear model reduction for binary distillation," IFAC Proceedings Volumes,
- vol. 19, no. 15, pp. 123–128, 1986.
- ₆ [20] W. Marquardt and M. Amrhein, "Development of a linear distillation model from design data for
- process control," Computers & Chemical Engineering, vol. 18, pp. S349–S353, 1994.
- 8 [21] A. Kienle, E. Stein, A. Rehm, and E. Kloppenburg, "Low-order dynamic models for two coupled
- distillation columns," in 1999 European Control Conference (ECC), IEEE, 1999.
- 10 [22] J. E. Cuthrell and L. T. Biegler, "On the optimization of differential-algebraic process systems,"
- 11 AIChE Journal, vol. 33, no. 8, pp. 1257–1270, 1987.
- 12 [23] L. S. Balasubramhanya and F. J. Doyle, "Nonlinear control of a high-purity distillation column using
- a traveling-wave model," AIChE Journal, vol. 43, no. 3, pp. 703–714, 1997.
- 14 [24] G. Zhu, "Low-order dynamic modeling of cryogenic distillation columns based on nonlinear wave
- phenomenon," Separation and Purification Technology, vol. 24, no. 3, pp. 467–487, 2001.
- ¹⁶ [25] S. Bian, M. A. Henson, P. Belanger, and L. Megan, "Nonlinear state estimation and model predictive
- control of nitrogen purification columns," Industrial & Engineering Chemistry Research, vol. 44,
- no. 1, pp. 153–167, 2005.
- ¹⁹ [26] S. Grüner, S. Schwarzkopf, I. Uslu, A. Kienle, and E. Gilles, "Nonlinear model predictive control of
- multicomponent distillation columns using wave models," IFAC Proceedings Volumes, vol. 37, no. 1,
- pp. 215–220, 2004.
- [27] S. Schwarzkopf, Echtzeitfahige optimierungsbasierte Regelung von Stofftrennprozessen. PhD thesis,
- Otto-von-Guericke-Universitat Magdeburg, 2012.
- ²⁴ [28] N. Hankins, "A non-linear wave model with variable molar flows for dynamic behaviour and dis-
- turbance propagation in distillation columns," Chemical Engineering Research and Design, vol. 85,
- no. 1, pp. 65–73, 2007.
- 27 [29] Y. Fu and X. Liu, "Nonlinear wave modeling and dynamic analysis of high-purity heat integrated
- air separation column," Separation and Purification Technology, vol. 151, pp. 14–22, 2015.
 - ©A. Caspari et al. 29 Page 29 of 33

- [30] L. Cong, L. Chang, and X. Liu, "Nonlinear-wave based analysis and modeling of heat integrated distillation column," Separation and Purification Technology, vol. 150, pp. 119–131, 2015.
- [31] Y. Fu and X. Liu, "An advanced control of heat integrated air separation column based on simplified wave model," *Journal of Process Control*, vol. 49, pp. 45–55, 2017.
- [32] A. Caspari, C. Offermanns, P. Schäfer, A. Mhamdi, and A. Mitsos, "A flexible air separation process:
- 2. optimal operation using economic model predictive control," AIChE Journal, vol. 65, no. 11, 2019.
- [33] R. Huang, V. M. Zavala, and L. T. Biegler, "Advanced step nonlinear model predictive control for air separation units," J. Process Control, vol. 19, no. 4, pp. 678–685, 2009.
- [34] T. Johansson, "Integrated scheduling and control of an air separation unit subject to time-varying
 electricity prices," Master's thesis, KTH Royal Institute of Technology, Department of Chemical
 Engineering and Technology, 2015.
- [35] A. U. Raghunathan and L. T. Biegler, "Mathematical programs with equilibrium constraints
 (MPECs) in process engineering," Computers & Chemical Engineering, vol. 27, no. 10, pp. 1381–1392,
 2003.
- [36] J. B. Rawlings, D. Q. Mayne, and M. M. Diehl, Model Predictive Control: Theory, Computation,
 and Design, 2nd Edition. Nob Hill Publishing, LLC, 2017.
- 17 [37] Analytic Sciences Corporation, Applied Optimal Estimation. MIT Press Ltd, 1974.
- [38] V. Becerra, P. Roberts, and G. Griffiths, "Applying the extended kalman filter to systems described by nonlinear differential-algebraic equations," Control Engineering Practice, vol. 9, no. 3, pp. 267–281, 2001.
- [39] Functional Mock-up Interface for Model Exchange and Co-Simulation, "https://fmi-standard.org/," accessed 2019.
- ²³ [40] R. G. Brusch and R. H. Schapelle, "Solution of highly constrained optimal control problems using nonlinear programing," *AIAA Journal*, vol. 11, no. 2, pp. 135–136, 1973.
- [41] R. W. H. Sargent and G. R. Sullivan, "The development of an efficient optimal control package," in
 Optimization Techniques, pp. 158–168, Springer-Verlag, 1978.
- ²⁷ [42] L. T. Biegler, Nonlinear Programming: Concepts, Algorithms, and Applications to Chemical Pro-²⁸ cesses. SIAM, 2010.

©A. Caspari et al. 30 Page 30 of 33

- [43] A. Caspari, J. M. M. Faust, F. Jung, C. Kappatou, S. Sass, Y. Vaupel, R. Hannesmann-Tamás,
- A. Mhamdi, and A. Mitsos, "Dyos a framework for optimization of large-scale differential algebraic
- equation systems," Computer-Aided Chemical Engineering, vol. 46, 2019.
- ⁴ [44] R. Hannemann, W. Marquardt, U. Naumann, and B. Gendler, "Discrete first- and second-order
- adjoints and automatic differentiation for the sensitivity analysis of dynamic models," Procedia
- 6 Comput. Sci., vol. 1, no. 1, pp. 297–305, 2010.
- ⁷ [45] P. E. Gill, W. Murray, and M. A. Saunders, "SNOPT: An SQP algorithm for large-scale constrained optimization," SIAM Rev., vol. 47, no. 1, pp. 99–131, 2005.
- 9 [46] FilterPy, "https://filterpy.readthedocs.io/," accessed 2019.
- 10 [47] H.-W. Häring, ed., Industrial Gases Processing. Wiley-VCH Verlag GmbH & Co. KGaA, 2007.
- 11 [48] F. G. Kerry, Industrial Gas Handbook: Gas Separation and Purification. CRC PR INC, 2007.
- [49] B. Daryanian, R. E. Bohn, and R. D. Tabors, "Optimal demand-side response to electricity spot prices for storage-type customers," *IEEE Power Eng. Rev.*, vol. 9, no. 8, pp. 36–36, 1989.
- [50] A. Ghobeity and A. Mitsos, "Optimal time-dependent operation of seawater reverse osmosis," Desalination, vol. 263, no. 1-3, pp. 76–88, 2010.
- [51] D. W. Green and R. H. Perry, "Perry's chemical engineers' handbook," Choice Reviews Online,
 vol. 45, no. 08, pp. 45–4393–45–4393, 2008.
- [52] R. C. Pattison, C. R. Touretzky, T. Johansson, I. Harjunkoski, and M. Baldea, "Optimal process operations in fast-changing electricity markets: Framework for scheduling with low-order dynamic models and an air separation application," *Industrial & Engineering Chemistry Research*, vol. 55, no. 16, pp. 4562–4584, 2016.
- [53] M. Morari and U. Maeder, "Nonlinear offset-free model predictive control," Automatica, vol. 48,
 no. 9, pp. 2059–2067, 2012.
- ²⁴ [54] C. Tsay, A. Kumar, J. Flores-Cerrillo, and M. Baldea, "Optimal demand response scheduling of an industrial air separation unit using data-driven dynamic models," *Computers & Chemical Engineering*, vol. 126, pp. 22–34, 2019.
- ²⁷ [55] G. Pannocchia, M. Gabiccini, and A. Artoni, "Offset-free MPC explained: novelties, subtleties, and applications," *IFAC-PapersOnLine*, vol. 48, no. 23, pp. 342–351, 2015.

©A. Caspari et al. 31 Page 31 of 33

- [56] A. Marchetti, B. Chachuat, and D. Bonvin, "Modifier-adaptation methodology for real-time optimization," Industrial & Engineering Chemistry Research, vol. 48, no. 13, pp. 6022–6033, 2009.
- [57] A. Caspari, Y. M. Perez, C. Offermanns, P. Schäfer, A.-M. Ecker, A. Peschel, F. Schliebitz, G. Zapp,
- A. Mhamdi, and A. Mitsos, "Economic nonlinear model predictive control of multi-product air
- separation processe," Computer-Adided Chemical Engieering, vol. 46, 2019.
- 6 [58] A. Caspari, C. Offermanns, P. Schäfer, A. Mhamdi, and A. Mitsos, "A flexible air separation process:
- 1. design and steady-state optimizations," AIChE Journal, vol. 65, no. 11, 2019.
- 8 [59] S. Grüner and A. Kienle, "Equilibrium theory and nonlinear waves for reactive distillation columns
- and chromatographic reactors," Chemical Engineering Science, vol. 59, no. 4, pp. 901–918, 2004.

A Dynamic Offline Optimization using Constant Holdup Wave

Propagation Model

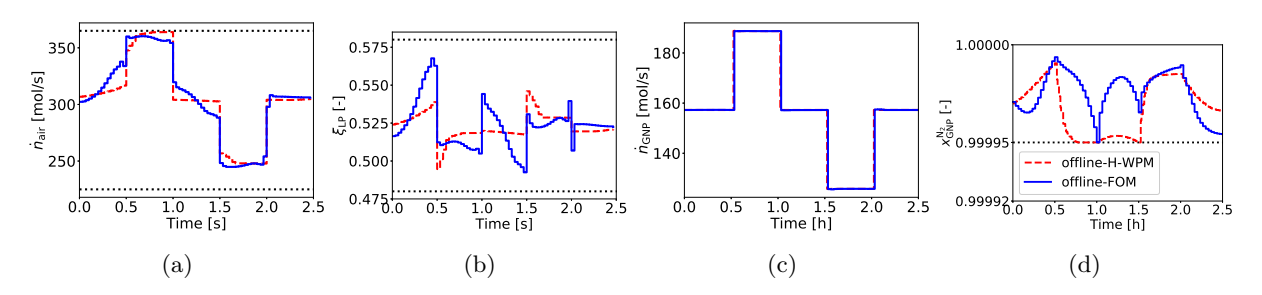


Fig. 11: Control and state variable profiles from offline optimization with FOM and H-WPM. State profiles result from FOM by simulation with the control variable profiles resulting from the optimization with FOM and H-WPM. The control variable profiles are piecewise constantly discretized with 2 minutes intervals. Bounds black dotted. (a) Air feed stream (control variable). The mean error between the two profiles is 1.9 %. (b) Column splitfactor (control variable). The mean error between the two profiles is 1.8 %. (c) Column product stream (state variable). (d) Column product concentration (state variable).

- 12 We compare the performance of the TWPM with the performance of the reduced column model with
- constant holdups as proposed by [1]. In [21], constant volume is assumed for each stage, which requires
- the volume calculation for every column stage. We therefore do not consider the constant volume model
- 15 here due to the increased computational demand. We denote the constant holdup model of [1] as H-WPM.
- 16 We perform the same case study as in Section 3.4.1 with the H-WPM. Fig. 11 shows the results. The
- control variable accuracy of the H-WPM with respect to the FOM is slightly worse than the accuracy of
- the TWPM (Section 3.4.1).

©A. Caspari et al. 32 Page 32 of 33

- We also perform the closed-loop case studies with the model of [1]. The results with the H-WPM and
- the TWPM are very similar, which is due to the feedback and the EKF. However, this could change, if
- we had an application with the liquid outlet stream or the column hold up appearing in the objective
- 4 function or the constraints. In this case, we would expect a better performance of the TWPM than the
- 5 H-WPM due to the variable holdup.

©A. Caspari et al. 33 Page 33 of 33